Chapter 2

Effects of Core and Cladding on Optical Guidance Properties of Holey Fibers

Jeong Kim

Additional information is available at the end of the chapter

http://dx.doi.org/10.5772/48280

1. Introduction

Optical fibers work as one of the most important parts for data transmission medium and light-signal processing component in optical communications. Microstructure holey optical fibers (MHOFs) from very new advanced technology have attracted considerable attention in research communities during recent years for the purpose of enhancing the performance of existing optical communication system [1-5]. Basically, the MHOFs can be made of a single material, in contrast to all other types of conventional optical fibers, which are normally manufactured with two or more materials. Only by properly designing the geometrical structures of the MHOF, numerous novel properties, such as single mode operation over the entire wavelength range of interest, zero or anomalous group-velocity dispersion, and large effective area, can be obtained. Moreover, various combinations of material composition in the MHOF may offer more opportunities for new and reliable fiber-optic devices.

Since the invention of the MHOFs, lots of applications have been explored and realized recently. Some of the novel applications include second-harmonic generation with broader bandwidth compared to some conventional fibers, polarization-preserving capability with elliptical air holes, fiber lasers, nonlinear-optic devices, and even highly sensitive fiber sensors. This special optical fiber, which is different from the conventional step-index fiber or graded-index fiber, can be fabricated by changing multiple parameters such as the diameter of each small air hole, its shape and location coordinates, the spacing between the adjacent holes, and the number of air-hole cladding layers. Because of the structural uniqueness, the MHOF can be designed to provide small or nearly constant dispersion and highly nonlinearity with single-mode operation characteristic over a wide wavelength range in optical communications.

In this chapter, following a brief review about the principle of light-guiding of the conventional optical fiber, general features of the MHOF will be introduced in section 3.

Showing the arrangement method of small-hole cladding on a transverse plane, modelling of the MHOF without and with an air core is addressed. For the electromagnetic analysis of the proposed microstructures with complicated geometries, the utilizations of a finite difference method (FDM) and a finite-difference time-domain (FDTD) technique are considered in the investigation of optical guidance properties, such as normalized propagation constant, mode field distribution, effective area, and chromatic dispersion. Employing the two numerical methods provides cross-verification and additive confidence in the accuracy of the results. Based on the FDTD and the FDM techniques, how the cladding structure of the HMOF affects optical guidance properties are analyzed in section 4. Then the investigation is extended to find out the effects of the size and shape of the core in the holey fiber on optical propagation properties in section 5.

2. Principle of optical guidance

Normally, optical fibers as cylindrical dielectric waveguides consist of core and cladding regions with at least two or more materials. Each region can be made of silica glass or other transparent materials such as plastic. Although practical optical fibers have several or a few layers of cylindrical cladding regions with cross-sectional ring shapes uniform along the light-travelling direction, these cladding regions can be functionally combined together and represented by the average cladding refractive index. The refractive index difference between the core and cladding can provide light confinement and hence guidance of light signal along the fiber. Upon travelling through the fiber, the optical signal is both attenuated and distorted. These effects impose a limit on how far the signal can travel in a fiber before it degrades beyond an acceptable level. The wavelength (λ) of operation is an important consideration in fiber-optic communication systems. Practical fiber optic systems operate in a wavelength range of 0.8 μm to 1.6 μm, where glass attenuation is low. In particular, the silica glass fiber exhibits local minimums in the spectral attenuation curve at 1.3-μm and 1.55-μm regions, which are often referred to as the transmission windows. Many commercial fiber-optic communication systems are designed for operation at these two wavelengths.

Optical fibers, as any other electromagnetic waveguide, can support discrete modes of propagation [6]. Assuming the cladding is just air instead of the multiple cylindrical cladding layers with respective material parameters, a simplified step-index optical fiber can be considered as shown in Figure 1(a). For more specific values, the simplified step-index waveguide has a core radius (a) of 1.0 μm, core refractive index (n_1) of 1.45, and cladding refractive index of 1.0. Then total internal reflection due to the difference between the core refractive index and the average cladding index can contribute to optical light guidance in the fiber. Analytical approach to calculate guided light propagation characteristics involves the method of separation of variables and the boundary conditions. For circularly cylindrical waveguides, the radial dependence of electromagnetic fields is governed by the Bessel differential equation, hence the solutions are described in terms of the Bessel and the modified Bessel functions. Figure 1(b) compares the effective refractive index ($\bar{\beta}$) of the fundamental mode obtained from the exact analytical solution and a numerical technique. The numerical approach will be described in the following section.

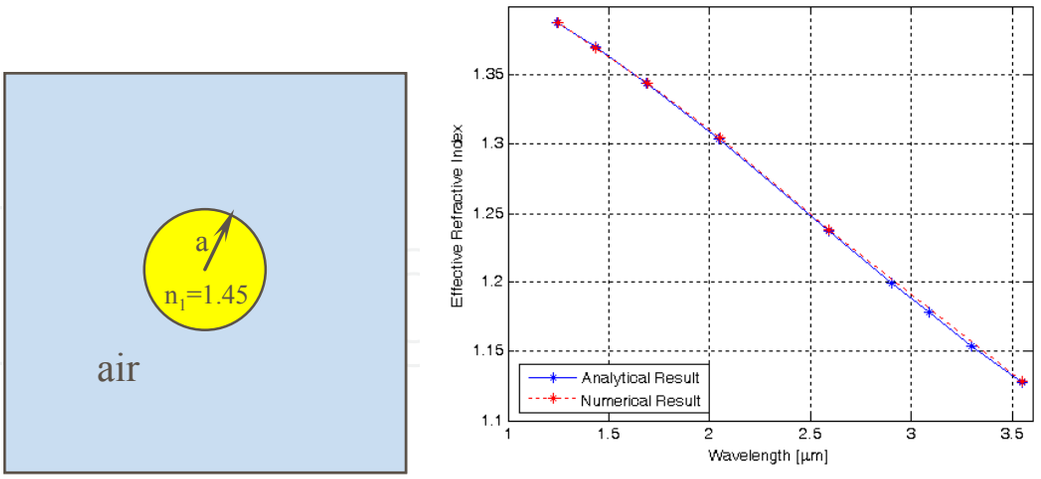

(a) (b)

Figure 1. (a) Simplified step-index optical fiber rod, (b) comparison of normalized propagation constants of the fundamental mode in the fiber of (a)

Based on the analytical and numerical results of the normalized propagation constants, it is reasonably found that the dielectric rod waveguide supports the first four modes at λ = 1.3 μm, which agrees well with the results from the Gloge's mode chart for this waveguide. And transverse electric field distributions, Ex and Ey, can be obtained by using the numerical method. Figure 2 illustrates the normalized field distributions of the first two modes for the optical rod waveguide at the operating wavelength of 1.3 μm. Here, it is noted that the side length of each square cell for the numerical analysis is 0.1 μm.

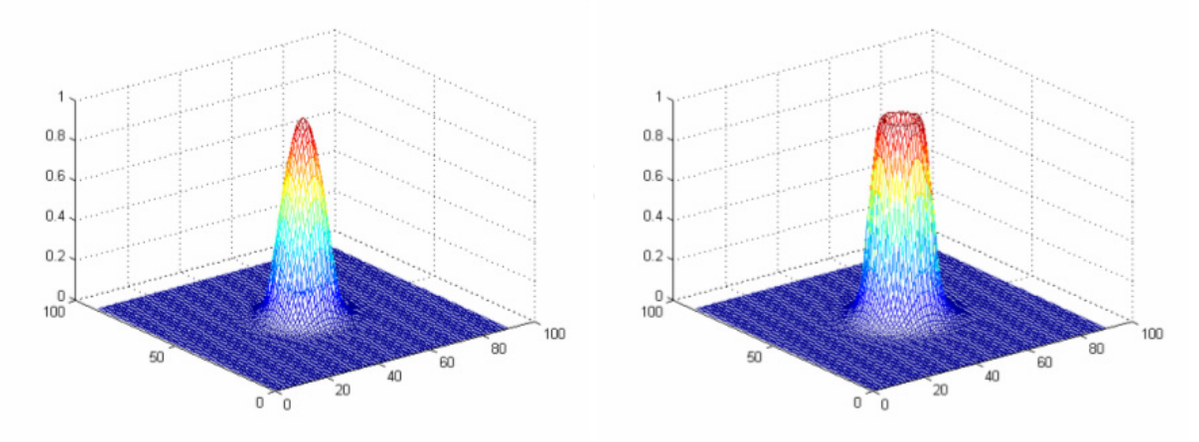

(a) (b)

Figure 2. Normalized field distributions of the first two modes for the optical rod fiber

Once the electric field distribution has been determined, the effective core area for the fundamental mode can be obtained using the following expression [7]:

$$A_{eff} = \frac{\left(\int_{-\infty}^{\infty} \int_{-\infty}^{\infty} |\mathbf{E}(x,y)|^2 \, dxdy \right)^2}{\int_{-\infty}^{\infty} \int_{-\infty}^{\infty} \left|\mathbf{E}(x,y)\right|^4 dxdy} \quad (1)$$

where $\mathbf{E}(x,y)$ is the electric field on a transverse plane. For the optical waveguide of Figure 1(a), the results of the effective area are 1.7925 μm², 2.0624 μm², and 2.2148 μm² at the wavelengths of 0.8 μm, 1.3 μm, and 1.55 μm, respectively.

3. FDTD and FDM algorithms for the MHOF analysis

Optical light is electromagnetic wave in nature, and thus its propagation properties are governed by the laws of electrodynamics which are collectively known as Maxwell's equations. It is known that guiding of light signals in the MHOF with photonic bandgap structures relies on constructive interference effect due to the periodic arrangement of identical air holes. On the other hand, when the air holes become random in size, location, or both, the phenomenon of total internal reflection takes place and the index difference between the core and cladding provides light confinement and hence guidance of light along the fiber. Although the propagation characteristics of complicated structures like arbitrary MHOFs cannot be calculated easily using analytical methods, there are ways to solve electromagnetic problems numerically.

In this section, two numerical techniques of finite-difference time-domain (FDTD) and finite difference method (FDM) are addressed considering extension to the analysis of holey optical fibers with arbitrary air-hole distributions. Each of these techniques has certain advantages. Using the FDTD method, the continuous electromagnetic field in a finite volume of space is sampled at distinct points in a space lattice and at equally spaced sampling points in time. The sampled data at the points are used for numerical calculations of allowed modes, without generating spurious mode solutions, in a given waveguide. Despite being an effective technique for calculation of propagation constants of guided modes, the FDTD method is not well suited for the evaluation of individual mode field distributions. This is because the source is an impulse function in the time domain covering an infinite spectrum, thus field-distribution solutions are superposition of all possible modes. To alleviate this problem with propagation constants available from FDTD, individual mode field distributions are obtained using the FDM, which can quickly and conveniently provide individual mode field solutions.

The FDTD has gained considerable popularity in recent years, because this method provides robust solutions, based on Maxwell's equations [8], and can readily accommodate complex-valued material properties. An arbitrary material object can be approximated by building up unit cells for which field component positions are disposed with the desired values of permittivity and permeability. Once the geometry of the object is specified in the numerical simulation region, source condition is modelled somewhere in the region. Initially, it is

assumed that all fields within the calculation domain are identically zero. Then, an incident wave is enforced to enter the numerical calculation region.

Using the MKS system of units, let us first consider Maxwell's curl equations expressed as:

$$\nabla \times \mathbf{E} = -\mu \frac{d\mathbf{H}}{dt} \tag{2}$$

$$\nabla \times \mathbf{H} = \varepsilon \frac{d\mathbf{E}}{dt} \tag{3}$$

where ε is the electrical permittivity constant in F/m and μ is the magnetic permeability constant in H/m. Expanding the curl expressions and equating the like components, the system of six coupled partial differential equations are formed for the FDTD analysis of electromagnetic wave interactions with general three-dimensional objects. It should be noted that the electric and magnetic field components (Ex, Ey, Ez, Hx, Hy, and Hz) are inter-related. That is, Maxwell's equations do not directly yield electric and magnetic field values, but rather relate the rate of change between electric and magnetic field values.

Adopting central finite difference approximation for space and time derivatives with accuracy to the second order, the following approximations as representative examples in a three dimensional (3D) FDTD formulation can be developed:

$$E_x^{n+1}(i+\tfrac{1}{2},j,k) = E_x^{n}(i+\tfrac{1}{2},j,k) + \frac{\Delta t}{\varepsilon_0 \varepsilon_r (i+\tfrac{1}{2},j,k)} \left\{ \left[\frac{H_z^{n+1/2}(i+\tfrac{1}{2},j+\tfrac{1}{2},k) - H_z^{n+1/2}(i+\tfrac{1}{2},j-\tfrac{1}{2},k)}{\Delta y} \right] - \left[\frac{H_y^{n+1/2}(i+\tfrac{1}{2},j,k+\tfrac{1}{2}) - H_y^{n+1/2}(i+\tfrac{1}{2},j,k-\tfrac{1}{2})}{\Delta z} \right] \right\} \tag{4}$$

$$H_y^{n+1/2}(i+\tfrac{1}{2},j,k+\tfrac{1}{2}) = H_y^{n-1/2}(i+\tfrac{1}{2},j,k+\tfrac{1}{2}) + \frac{\Delta t}{\mu} \left\{ \left[\frac{E_z^{n}(i+1,j,k+\tfrac{1}{2}) - E_z^{n}(i,j,k+\tfrac{1}{2})}{\Delta x} \right] - \left[\frac{E_x^{n}(i+\tfrac{1}{2},j,k+1) - E_x^{n}(i+\tfrac{1}{2},j,k)}{\Delta z} \right] \right\} \tag{5}$$

$$H_z^{n+1/2}(i+\tfrac{1}{2},j+\tfrac{1}{2},k) = H_z^{n-1/2}(i+\tfrac{1}{2},j+\tfrac{1}{2},k) + \frac{\Delta t}{\mu} \left\{ \left[\frac{E_x^{n}(i+\tfrac{1}{2},j+1,k) - E_x^{n}(i+\tfrac{1}{2},j,k)}{\Delta y} \right] - \left[\frac{E_y^{n}(i+1,j+\tfrac{1}{2},k) - E_y^{n}(i,j+\tfrac{1}{2},k)}{\Delta x} \right] \right\} \tag{6}$$

where i, j, k, and n are integers for Δx, Δy, Δz, and Δt, respectively, as the space and time increments [9].

Since optical fibers such as MHOFs generally have no variations along the direction of propagation and variations of material properties are limited to the transverse directions as shown in Figure 3, the 3D FDTD formulation can be simplified to the compact two dimensional (2D) FDTD algorithm [10]. By using phasor notation with the axial propagation constant (β), the first-order partial derivatives with respect to z are replaced with -jβ, because the z-dependence of fields is as exp(-jβz). And two adjacent fields required for the first-order derivatives in the discretized space region can be represented by a field at the mid point between them. Based on these two facts, the following formulation as an example is obtained:

$$H_y^{n+1/2}(i+\tfrac{1}{2},j) = H_y^{n-1/2}(i+\tfrac{1}{2},j) + \frac{\Delta t}{\mu}\left\{\left[\frac{E_z^n(i+1,j)-E_z^n(i,j)}{\Delta x}\right] + j\beta \cdot E_x^n(i+\tfrac{1}{2},j)\right\} \quad (7)$$

The resulting 2D algorithm takes advantage of significant reduction in the required computer memory allocation and running time. Thus, for computer-calculation of arbitrary waveguides that are uniform along the direction of wave propagation, only modelling of the cross sections of waveguides is sufficient.

Along with this efficient algorithm, infinite media in the 2D space for an arbitrary electromagnetic object need to be modelled carefully, because computer memory is limited in the calculation region even with advanced current technology. In order to model regions extending to infinity, a perfectly matched layer (PML) as a highly effective absorbing boundary condition (ABC) is designed at the outer lattice boundary of a calculation domain. Ideally, the absorbing medium is only as thick as a few lattice cells, highly absorbing, reflectionless to all impinging waves, and effective over the full range of operating wavelengths.

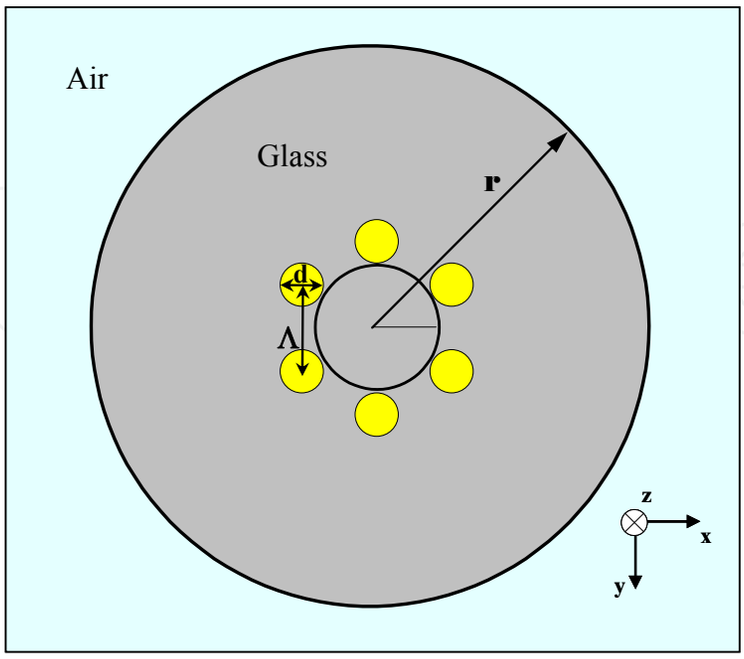

Figure 3. Schematic of a cross section for an MHOF with one layer of air holes in a hexagonal arrangement

Similarly to the development of the FDTD algorithm, the FDM formulation can be derived from the coupled Maxwell's equations [8]. For continuous waves in linear and isotropic media, combining Eqs (2) and (3) results in the following vectorial wave equation:

$$\nabla \times \nabla \times \mathbf{E} - n^2 k_0^2 \mathbf{E} = 0 \tag{8}$$

where n is the refractive index and k_0 is the propagation constant in free space. Many waveguiding devices, like optical fibers, can be viewed as z-invariant, or piecewise z-invariant structures. For those structures, the refractive index n(x,y,z) varies slowly along the propagation direction z, which is valid for most photonic guided-wave devices. By using the vector identity of $\nabla \times \nabla \times = \nabla\left(\nabla \cdot\right) - \nabla^2$, Eq (8) can be written as

$$\nabla^2 \mathbf{E} + n^2 k_0^2 \mathbf{E} = \nabla\left(\nabla \cdot \mathbf{E}\right) \tag{9}$$

Also with the reasonable assumption of negligible time dependency along the z-axis, the FDM formulation as in Eq (9) can be implemented by replacing spatial derivatives with finite difference approximations. Here, it is noted that the transverse component of (9) is

$$\nabla^2 \mathbf{E}_t + n^2 k_0^2 \mathbf{E}_t = \nabla_t \left(\nabla_t \cdot \mathbf{E}_t + \frac{\partial E_z}{\partial z} \right) \tag{10}$$

where the subscript "t" stands for the transverse components. Since the longitudinal component may be readily obtained by application of the following zero divergence (Gauss's law) constraint:

$$\nabla \cdot \left(n^2 \mathbf{E} \right) = 0, \tag{11}$$

the transverse components are sufficient to describe the full-vectorial natures of the electromagnetic field in an optical waveguide.

For the initial investigation of guidance properties of MHOFs, the optical fiber shown in Figure 3 is computer-analyzed. Generally, the MHOF geometry can be described with two parameters, pitch length (Λ) and diameter (d), as indicated in Figure 3. Here, the pitch length is the distance between centers of two closest air holes with the cylindrical shape. For the MHOF of Figure 3, each small air hole has a diameter of 1.4 μm, constituting a hexagon with Λ = 1.7 μm. The glass portion surrounding the six air holes of the yellow regions has a refractive index of 1.45. The outer radius (r) of the holey fiber is assumed to be 10 μm. Also, the outside region of the MHOF is air.

Once the cross section of a holey fiber is defined in a proper calculation domain, the FDTD simulation can be undertaken with several specified parameters, such as τ in defining a Gaussian source, Δt for stable simulation, the total number (n_{tot}) of time steps for sampling data in the time domain, and reasonable values of β. Here, in order to avoid numerical divergence and ensure stability of the FDTD algorithm, an appropriate Δt needs to be selected to satisfy the following stability condition:

$$\Delta t \le \frac{1}{c_M\left[\frac{1}{\Delta x^2}+\frac{1}{\Delta y^2}+\frac{1}{\Delta z^2}\right]^{1/2}} \tag{12}$$

where c_M is the maximum wave phase velocity within a given numerical model. Summarizing the mechanism behind the FDTD analysis, the computer simulation proceeds by the following steps:

- Choose appropriate parameter values (τ, Δt, n_{tot}, and β)
- Data sampling of a field component in the time domain
- Take the Fourier transform of the time data
- Get spectral data of a field component
- Pick mode frequencies associated with the β value
- Collect β and mode frequency data
- Make a plot of mode index versus wavelength

Figure 4 illustrates the characteristic curves, which are obtained from the FDTD calculation, for the first three lower-order modes of the MHOF defined in Figure 3.

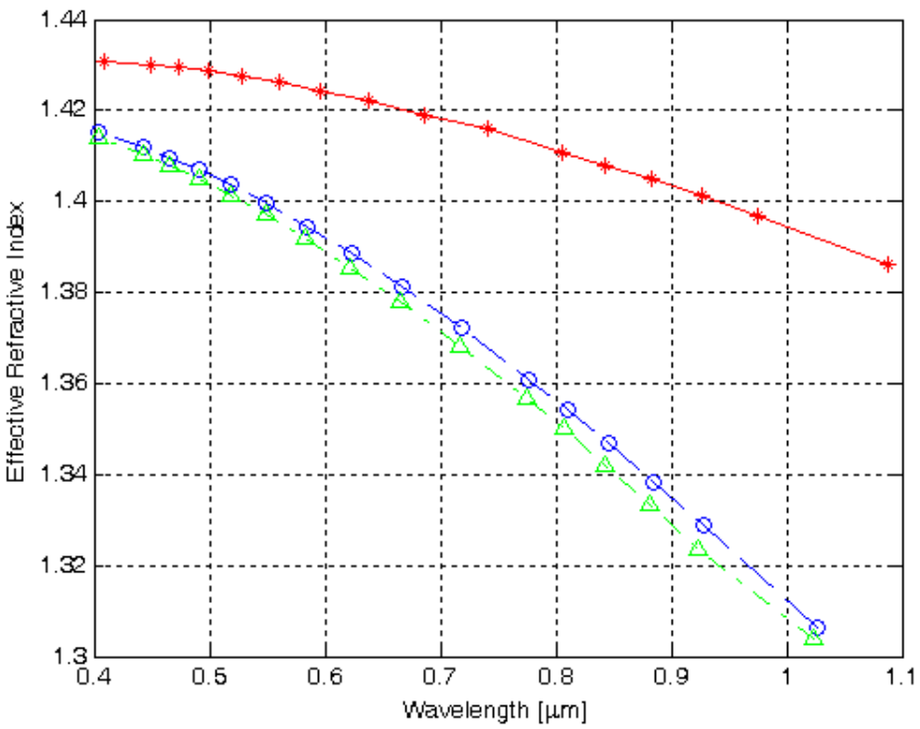

Figure 4. Effective refractive index versus wavelength for the first three modes in an MHOF with one layer of air holes

The red curve with the star symbols plots the normalized propagation constant for the first mode versus wavelength, while the blue and green curves show the normalized propagation constants for the second and the third modes, respectively. The results indicate

that the HMOF with a single hexagonal air-hole cladding layer supports multimode guiding.

4. Effects of cladding structure on optical guidance properties

Based on the FDTD and the FDM techniques, important optical guidance properties of the fundamental mode, such as normalized propagation constant, chromatic dispersion, field distributions, and effective area, have been investigated for the HMOF with different structural parameter values. In this section, how the cladding structure of the HMOF affects optical guidance properties is first analyzed. Then in the next section, the investigation is extended to find out the effects of the core in the holey fiber design on optical propagation properties.

For the case when the MHOF has Λ = 2.0 μm, d = 1.2 μm, and r = 12.0 μm with three hexagonal cladding layers of air holes as in Figure 5, the effective refractive index characteristics are computer-calculated by the FDTD analysis approach. Assuming that the core index, which is the same as the surrounding medium of the small air holes, is 1.45 and the geometry of the MHOF is uniform along the z-axis, Figure 6 shows the results for the effective refractive index of the fundamental mode obtained from the FDTD method without accounting for the material dispersion (D_{mat}). In this analysis, a Gaussian pulse source, which excites the MHOF at one end, is used with the parameter value of $\tau = 0.25 \times 10^{-6}$. The expression describing the source is given as

$$S_G = \exp\left[-\frac{(x^2 + y^2)}{2\tau^2}\right] \tag{13}$$

where x and y are perpendicular coordinates in the transverse plane on a cross section of the holey fiber. In Figure 6, the 3D plot of the source is also shown inset.

In order to see the effect of the thickness of the dielectric layer surrounding the air holes, the outer radius (r) of the holey fiber is reduced from 12 μm to 9 μm. As shown in Figure 6, no significant change on the propagation constant occurs. The propagation constants for the 12-μm and 9-μm radius MHOFs are almost the same except for the longest wavelength. The reason is that the field of the fundamental mode is nearly entirely confined to a region of 9-μm radius, which is about 6 times the operating wavelength of λ = 1.55 μm. It should be also noted that both of the MHOFs allow only a single mode over the wavelength range from 0.9 μm to 1.8 μm.

Now, with the same parameter values (Λ = 2.0 μm and d = 1.2 μm) as in Figure 5, the MHOF is numerically analyzed by changing the number of hexagonal air-hole cladding layers. Since it is demonstrated that increasing the outer radius (r) about 6 times larger than the operating wavelength doesn't affect the propagation characteristics significantly, the dielectric glass material surrounding the air holes has been assumed to have the enough thickness. Here, however, it is assumed that the high-index material of the MHOF is pure fused silica (100 mol % SiO_2) with refractive index n_1, while the low-index region is air. That

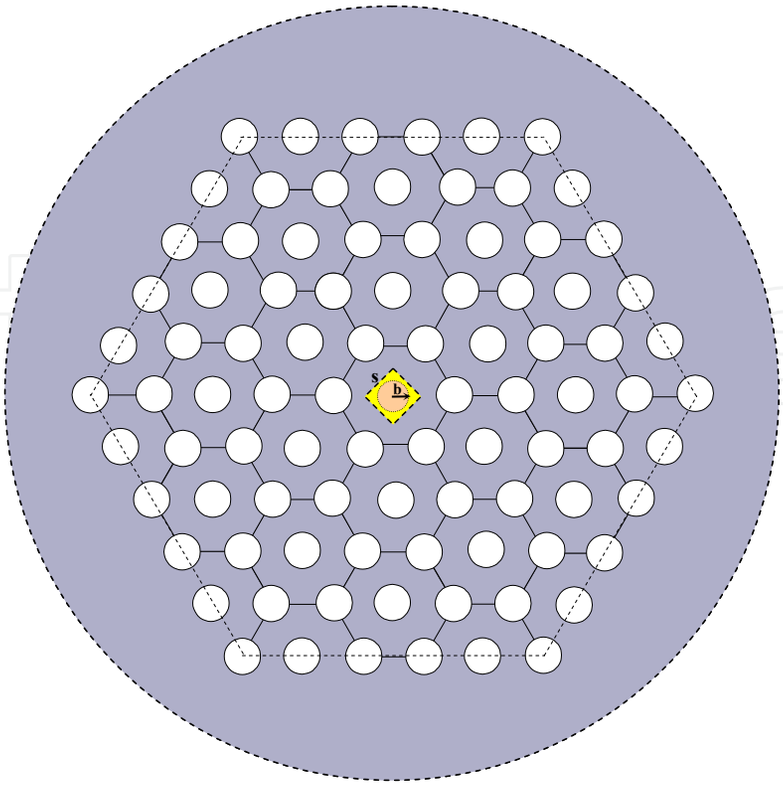

Figure 5. Transverse structure of the MHOF (The air holes in the fifth layer from the core are linked by the dashed line, forming a hexagonal ring.)

is, in order to account for the material dispersion effect of the glass [7], the wavelength dependence of the glass refractive index is directly incorporated in the effective index calculation through the following widely-utilized Sellmeier's equation:

$$n_1(\lambda) = \left[1 + \sum_{j=1}^{3} \frac{A_j \lambda^2}{\lambda^2 - \lambda_j^2}\right]^{1/2} \tag{14}$$

where material constants, A_j and λ_j, for the pure fused silica are given as ($A_1 = 0.6961663$, $\lambda_1 = 0.0684043$), ($A_2 = 0.4079426$, $\lambda_2 = 0.1162414$), and ($A_3 = 0.8974794$, $\lambda_3 = 9.8961610$).

Continuing numerical analysis for the optical guidance properties of the step-index rod fiber case, chromatic dispersion is calculated using the FDM analysis and compared to the exact analytical results. With the effective refractive index results in section 2, the chromatic dispersion (D_{ch}) can be calculated by using the following relationship:

$$D_{\text{ch}} = -\frac{\lambda}{c}\frac{d^2\overline{\beta}}{d\lambda^2} \tag{15}$$

where c is the speed of light in free space [6]. The comparison of the chromatic dispersion results is shown in Figure 7(a) for the dielectric rod waveguide. Here, the blue curve is from the analytical solution, while the red curve is obtained for the FDM analysis. It is noticed

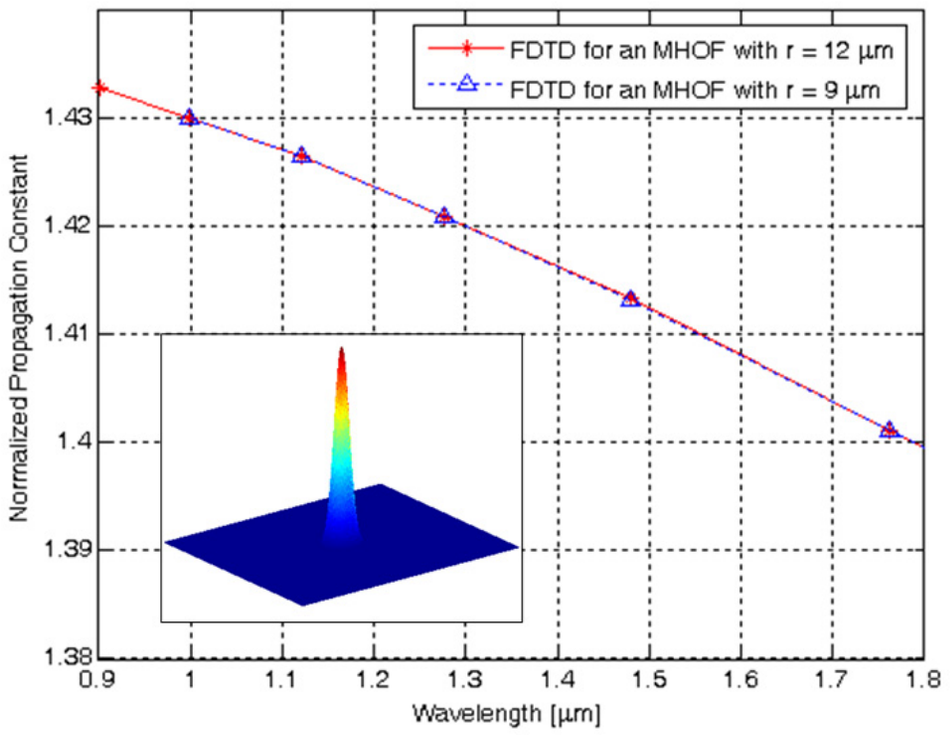

Figure 6. Normalized propagation constants of 3-layer MHOFs with different radii (Inset: Gaussian source for the FDTD analysis)

that the two results agree well. This provides additive confidence that the FDM analysis can accurately predict chromatic dispersion in holey fibers.

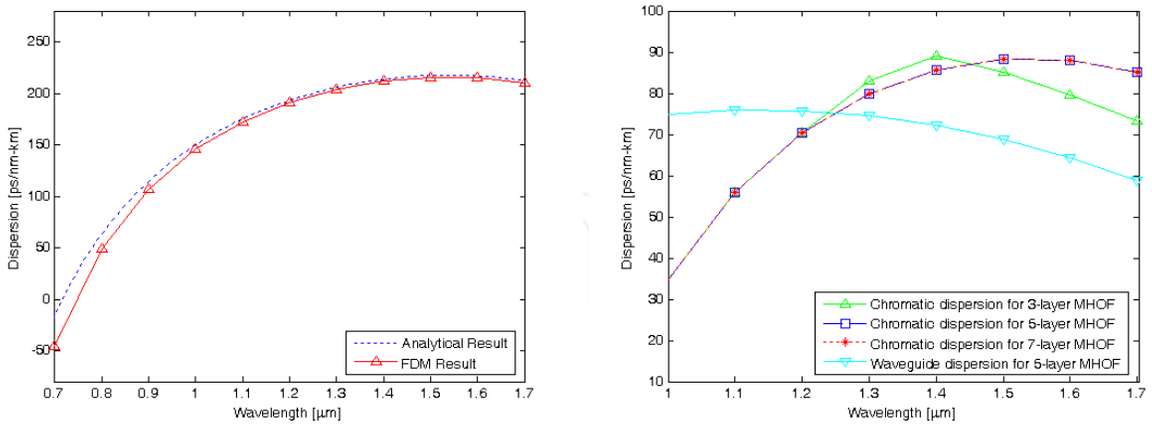

(a) (b)

Figure 7. Dispersion results: (a) for the dielectric rod waveguide of Figure 1(a), (b) for the MHOFs with Λ = 2.0 μm, d = 1.2 μm, and different numbers of air-hole cladding layers

Again for the MHOF shown in Figure 6, initially, the number of air-hole layers is chosen to be 5. The background glass material (n_1) is assumed to be pure fused silica with enough extension. The blue curve in Figure 7(b) shows the chromatic dispersion as a function of

wavelength for the fundamental mode in the MHOF with five hexagonal cladding layers of air holes. The cyan (light-blue) curve illustrates the waveguide dispersion for the same holey fiber without material dispersion included. Compared with the chromatic dispersion result, the waveguide dispersion varies rather gradually from about 78.985 ps/nm·km to 59.537 ps/nm·km over the wavelength range between 1.0 μm and 1.7 μm. It is noticed that the five-layer MHOF provides positive chromatic and waveguide dispersions over the same wavelength range.

When the number of hexagonal air-hole cladding layers is changed from 5 to 3, it is noticed that the chromatic dispersion curves for the both cases are very close at the shorter wavelength range but deviation occurs from 1.2 μm. However, with the increased number of air-hole layers to 7, the D_{ch} dispersion changes very close to the case of the five-layer MHOF. And adding more air-hole cladding layers like nine or eleven layers does not significantly change the chromatic dispersion result from the five-layer holey fiber in the operation wavelength of interest for general optical communications. This behaviour is reasonably attributed to the fact that when the operating wavelength is shorter, electromagnetic fields are more confined to the core region and only the core region has a major impact on the optical guidance properties. By comparison, when the operating wavelength is longer, fields spread more to the cladding region and the index profile of the cladding region has more influence on the effective refractive index.

Incorporating the material dispersion for the MHOF with five layers of air holes, the field solution of the fundamental mode is obtained by using the finite difference technique. For instance, Figure 8 illustrates the normalized field pattern for the Ex electric component of the MHOF at the operating wavelength of 1.55 μm. Figure 8(a) demonstrates the top view with the colorbar scale in the right side and Figure 8(b) does the 3D view. As expected, it is observed that most of the energy is confined within the core region. Also for the fundamental mode of the MHOF with three, seven or nine cladding layers of air holes, about the same field shape is maintained at the same wavelength.

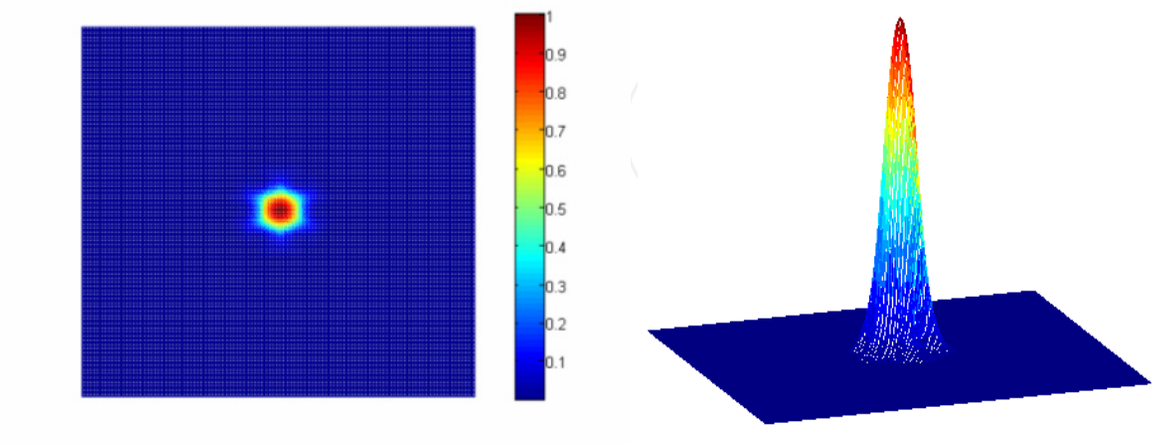

Figure 8. Normalized field pattern for the Ex electric component of the fundamental mode at λ = 1.55 μm in the MHOF with five layers of air holes and the parameter values of Λ = 2.0 μm and d = 1.2 μm: (a) top view with the colorbar scale; (b) 3D view

Furthermore, similarly to the results of optical guidance properties for the normalised propagation constant, chromatic dispersion, and field distribution, those for the effective core area also tend to change very little when the number of hexagonal air-hole cladding layers becomes larger than five. In other words, adding more air-hole layers to the cladding beyond a certain point will not significantly affect the propagation constant, dispersion, and, in fact, all guidance properties of the MHOF waveguide.

5. Effects of the central air core on optical guidance properties

For the MHOF defined with the geometrical parameters of Λ = 2.0 μm and d = 1.2 μm, and five cladding layers of air holes, how the core structure affects optical guidance properties is also investigated. By sizing the central air-hole radius (b) as shown in Figure 5, the MHOF with an air core is analyzed to obtain its propagation characteristics, based on FDM and FDTD methods for the full-vectorial analysis.

Getting the normalised propagation constant of the given optical fiber and computing its second derivative with respect to λ, dispersion characteristics can be evaluated. Figure 9 shows chromatic dispersion variations for the MHOF, as the radius of the central air hole is sized from 0 μm to 0.4 μm. This result indicates that the dispersion flatness can be achieved around 1.3-μm wavelength by designing the MHOF with b = 0.25 μm. Specifically, the chromatic dispersion (ps/nm·km) is -0.7724, 0.2635, -0.4532 at wavelengths of 1.2, 1.3, and 1.4 μm, respectively. This near-zero ultra-flattened dispersion is highly desirable in long-haul fiber-optic communication systems.

When the circular hole at the center is changed to the square air hole with the side length (s) of 0.4432 μm, which has the area equal to that of the former, the chromatic dispersion versus wavelength for the fundamental mode in the MHOF is also depicted as the green dashed line with the diamond symbols in Figure 9. As noticed, the chromatic dispersion curves for the both cases are close at the shorter wavelength range around 1.0 μm, compared to the gap between two curves at the wavelength range around 1.7 μm.

The effective area for the fundamental mode is also evaluated by using the field distribution results, as shown in Figure 10. The red dashed line represents the effective area for the MHOF at the operating wavelength of 1.3 μm and the blue solid line at 1.55 μm, as the radius of the core hole (b) is sized from 0 to 0.6 μm. It is noted that the effective core area tends to increase with the size of the central air hole at both the operation wavelengths. The reason is that with bigger core hole the electromagnetic fields spread further into the cladding region. Thus sizing the core hole provides a decent way to control the effective area. Also, notice that the effective areas at the longer wavelength of 1.55 μm generally result in larger values for each different hole radius, compared to those at 1.3 μm. While the effective area is 6.7926 μm^2 for the MHOF with s = 0.4432 μm at λ = 1.55 μm, as indicated by the dotted line, those with b = 0.25 μm at λ = 1.3 μm and 1.55 μm are 6.691 μm^2 and 7.145 μm^2, respectively.

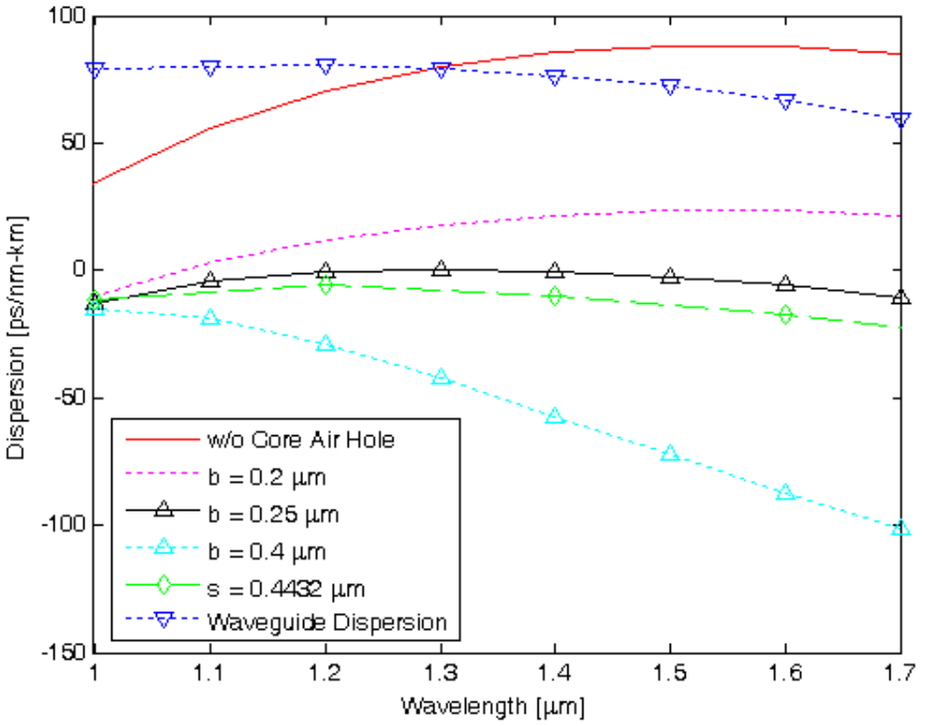

Figure 9. Chromatic and waveguide dispersions for the MHOF with the five layers of air holes, the parameter values of $\Lambda = 2.0$ μm and $d = 1.2$ μm, and different central core air holes

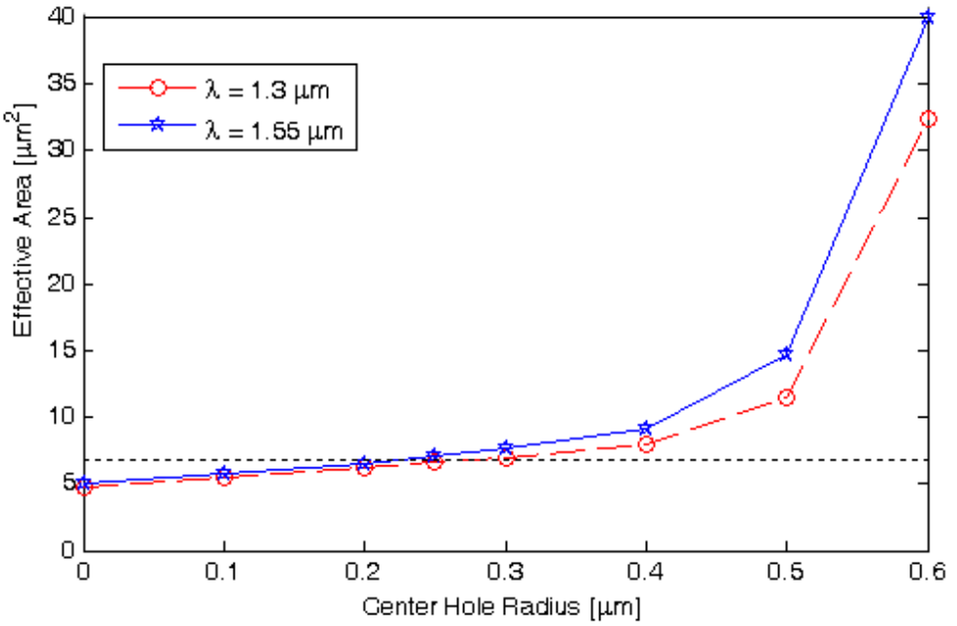

Figure 10. Effective area for the fundamental mode versus the radius of the central air hole for the same MHOF as given in Figure 9

6. Conclusions

For the investigation of optical guidance properties of MHOFs, two numerical techniques of the FDTD and FDM are employed, considering extension to the analysis of holey optical fibers with random hole distributions in terms of material, shape, size, or location [11]. In this investigation, it is found that the outer radius (r) of the MHOF with Λ = 2.0 μm, d = 1.2 μm, and the three hexagonal air-hole cladding layers doesn't affect the propagation characteristics significantly, if its thickness is about 6 times larger than the operating wavelength. And the 3-layer MHOF supports only a single mode over the wavelength range from 0.9 μm to 1.8 μm, whereas the MHOF with Λ = 1.7 μm, d = 1.4 μm, and the single hexagonal air-hole cladding layer multimode guiding.

In the case of the MHOF with Λ = 2.0 μm, d = 1.2 μm, and r = 12.0 μm, the guidance characteristics, such as normalized propagation constant, chromatic dispersion, mode field distribution, and effective area tend to change very little when the number of hexagonal air-hole cladding layers becomes larger than five. In other words, adding more hexagonal air-hole layers to the cladding beyond a certain point will not significantly affect the propagation constant, dispersion, and, in fact, all guidance properties of the MHOF waveguide.

By comparison, the size of the central core air hole has fair effect on the optical guidance properties of MHOFs. The MHOF with Λ = 2.0 μm, d = 1.2 μm, b = 0.25 μm, and the five hexagonal cladding layers provides -4.2647 ps/nm·km of chromatic dispersion and 7.145 μm^2 of effective area at λ = 1.55 μm. Similarly, the MHOF with the square air core of the equal area shows close results with -15.4055 ps/nm·km of the former and 6.7926 μm^2 of the latter. As a general guideline, when the operating wavelength is shorter, electromagnetic fields are more confined to the core region and only the core region has a major impact on the optical guidance properties. Conversely, when the operating wavelength is longer, fields spread more to the cladding region and the index profile of the cladding region has more influence on these.

Even thought the holey optical fibers have complicated geometries, which make the electromagnetic analysis difficult, the results in this investigation can be utilized as a general guide. And depending on the desired applications, the MHOF with various design parameters are expected to be useful for novel developments related to optical communication in many areas.

Author details

Jeong Kim
Chungnam National University, Department of Electric, Electronic and Communication Engineering Education, Daejeon, South Korea

Acknowledgement

This study was financially supported by research fund of Chungnam National University in 2010 and 2011.

7. References

[1] Knight, J.C.; Broeng, J.; Birks, T.A. & Russell, P.St.J. (1998). Photonic Band Gap Guidance in Optical Fibers. *Science,* Vol.282, (November 1998), pp. 1476-1478, ISSN 1095-9203

[2] Petrovic, J. (2008). Modelling of Long Period Gratings in Photonic Crystal Fibres and Sensors Based on Them, In: *Recent Advances in Modelling and Simmulation,* InTech, G. Petrone & G. Cammarata, (Ed.), pp. 417-432, ISBN 978-3-902613-25-7, Vienna, Austria

[3] Monro, T.M.; Richardson, D.J.; Broderick, N.G.R. & Bennet, P.J. (2000). Modeling Large Air Fraction Holey Optical Fibers. *Journal of Lightwave Technology,* Vol.18, No.1, (January 2000), pp. 50-56

[4] Ranka, J.K.; Windeler, R.S. & Stentz, A.J. (2000). Optical Properties of High-Delta Air Silica Microstructure Optical Fibers. *Optics Letters,* Vol.25, No.11, (June 2000), pp. 796-798

[5] Benabid, F.; Couny, F.; Knight, J.C.; Birks, T.A. & Russell, P.St.J. (2005). Compact, Stable and Efficient All-Fibre Gas Cells Using Hollow-Core Photonic Crystal Fibres. *Nature,* Vol.434, (March 2005), pp. 488-491, ISSN 0028-0836

[6] Keiser, G. (2010). *Optical Fiber Communications,* McGraw-Hill, ISBN 978-007-3380-71-1, New York, U.S.A.

[7] Agrawal, G.P. (2010). *Fiber-Optic Communication Systems,* Wiley, ISBN 978-047-0505-11-3, New York, U.S.A.

[8] Hayt, W.H.Jr. & Buck, J.A. (2011). *Engineering Electromagnetics,* McGraw-Hill, ISBN 978-007-3380-66-7, New York, U.S.A.

[9] Kim, J.I. (2007). Holey Fiber Analysis Employing FDM and FDTD Methods on the Transverse Plane. *Microwave and Optical Technology Letters,* Vol.49, No.7, (July 2007), pp. 1592-1594

[10] Taflove, A. & Hagness, S.C. (2005). *Computational Electrodynamics: the Finite-Difference Time-Domain Method,* Artech House, ISBN 978-158-0538-32-9, Boston, U.S.A.

[11] Pickrell, G.; Kominsky, D.; Stolen, R.; Ellis, F.; Kim, J.; Safaai-Jazi, A. & Wang, A. (2004). Microstructural Analysis of Random Hole Optical Fibers. *Photonics Technology Letters,* Vol.16, No.2, (February 2004), pp. 491-493